

# PHYSICS OF POLARIZED SCATTERING AT MULTI-LEVEL ATOMIC SYSTEMS

J. O. Stenflo<sup>1,2</sup>

<sup>1</sup>*Institute of Astronomy, ETH Zurich, CH-8093 Zurich, Switzerland*

<sup>2</sup>*Istituto Ricerche Solari Locarno, Via Patocchi, 6605 Locarno-Monti, Switzerland*

stenflo@astro.phys.ethz.ch

## ABSTRACT

The symmetric peak observed in linear polarization in the core of the solar sodium D<sub>1</sub> line at 5896 Å has remained enigmatic since its discovery nearly two decades ago. One reason is that the theory of polarized scattering has not been experimentally tested for multi-level atomic systems in the relevant parameter domains, although the theory is continually being used for the interpretation of astrophysical observations. A laboratory experiment that was set up a decade ago to find out whether the D<sub>1</sub> enigma is a problem of solar physics or quantum physics revealed that the D<sub>1</sub> system has a rich polarization structure in situations where standard scattering theory predicts zero polarization, even when optical pumping of the  $m$  state populations of the hyperfine-split ground state is accounted for. Here we show that the laboratory results can be modeled in great quantitative detail if the theory is extended to include the coherences in both the initial and final states of the scattering process. Radiative couplings between the allowed dipole transitions generate coherences in the initial state. Corresponding coherences in the final state are then demanded by a phase closure selection rule. The experimental results for the well understood D<sub>2</sub> line are used to constrain the two free parameters of the experiment, collision rate and optical depth, to suppress the need for free parameters when fitting the D<sub>1</sub> results.

*Subject headings:* line: profiles – methods: laboratory: atomic – polarization – radiation mechanisms: general – scattering – Sun: atmosphere

## 1. Introduction

The development of new theories will often go astray unless guided and tested by observations or experiments. In the early stages of quantum physics experiments with polarized scattering helped guide the development of the theory. The experiments by Wilhelm Hanle in Göttingen (Hanle 1924) led not only to the discovery of the well used Hanle effect but at the same time demonstrated the concept of coherent superposition of quantum states and the partial decoherence caused by external magnetic fields. The new quantum theory was built on these concepts.

The literature on experiments with the scattering of polarized light came to an abrupt end around 1935, apparently because the topic was

considered exhausted and less rewarding than other areas, and because the observed phenomena were believed to be sufficiently understood. The theoretical understanding covered the parameter domain accessible at that time, which in terms of polarimetric sensitivity was unbelievably crude in comparison with what is now possible with modern technology. Therefore the quantum scattering theory never got experimentally tested over a wide range of weak polarization phenomena that are accessible with current instrumentation. The theory is nevertheless being systematically applied for the interpretation of astrophysical observations in this untested parameter domain.

With the implementation in the 1990s of a new technology (ZIMPOL) in solar spectropolarimetry (Povel 1995, 2001; Gandorfer et al.

2004), which allowed the recording of the Sun’s spectrum with a polarimetric precision of  $10^{-5}$ , the linearly polarized spectrum (Stokes  $Q/I$ ) observed near the solar limb was found to be spectrally structured as the intensity spectrum, but the spectral structures were totally different, it was like uncovering a new spectral face of the Sun (Stenflo & Keller 1996, 1997). It is therefore referred to with the term ‘Second Solar Spectrum’, or with the acronym SS2 (implying that the ordinary intensity spectrum is SS1). The origin of this polarized spectrum is coherent scattering processes in the Sun’s atmosphere. Magnetic fields do not produce this spectrum, but they modify it — SS2 is a playground for the Hanle effect.

Through intense theoretical efforts most of these unfamiliar structures could be identified and understood within the framework of standard quantum scattering theory, revealing remarkable polarization signatures of quantum interference between states of different total angular momenta ( $J$  quantum numbers), hyperfine structure and isotope effects, optical pumping, molecular scattering, and partial frequency redistribution effects in polarized radiative transfer (cf. Stenflo 2004, for a review).

A culmination of the theoretical work to build a comprehensive quantum-mechanical foundation for the radiation-matter interactions occurred with the publication of the monumental monograph by Landi Degl’Innocenti & Landolfi (2004). A regular series of International Workshops has been devoted to the subject of ‘Solar Polarization’ since 1995, the latest, no. 7, in Kunming, China, September 2013 (Nagendra et al. 2014). The physics of polarized scattering has been a central topic of these Workshops.

In spite of these various efforts, one kind of observed feature in the Second Solar Spectrum has remained enigmatic and stubbornly resisted all attempts to explain it, namely the weak linear polarization peak observed at the center of the Na I  $D_1$  line at 5896 Å and the Ba II  $D_1$  line at 4934 Å (Stenflo et al. 2000a,b), although attention to the enigmatic sodium  $D_1$  feature was drawn already in the 1996 paper in *Nature* (Stenflo & Keller 1996). The problem is that  $D_1$  type lines, which have angular momentum quantum numbers  $J = 1/2$  for both the lower and upper atomic level is expected to be intrinsically unpolarizable, represent-

ing polarization ‘null’ lines. However, since both sodium and barium have nuclear spin  $3/2$ , both the lower and upper levels are split into hyperfine structure states with total angular momentum quantum numbers  $F = 1$  and  $2$ . A number of attempts have been made to explain the observed  $D_1$  polarization in terms of optical pumping of the hyperfine structure levels of the ground state (Landi Degl’Innocenti 1998; Casini et al. 2002; Casini & Manso Sainz 2005), but all of them have failed because the predicted  $D_1$  polarization is too small by about two orders of magnitude and has the wrong symmetry (anti-symmetric polarization profile instead of the observed symmetric one) (Trujillo Bueno et al. 2002; Kerkeni & Bommier 2002; Klement & Stenflo 2003).

To find out if this enigma is a problem of solar physics or of quantum physics, a laboratory experiment was set up to explore the polarization structure of  $D_1$  scattering under controlled conditions. The experiment unambiguously showed that there is indeed a problem with the quantum theory of polarized scattering, since the theory predicts null results when the experiment revealed a rich polarization structure (Thalmann et al. 2006, 2009).

In search for ways in which the theory of quantum scattering would need to be extended to explain what was seen in the laboratory experiment, it was realized that if coherences in *both* the initial *and* final ground states could be included in the theory for the scattering process, then the atomic system would possess a much richer resonant structure that would be able to generate polarization signatures of the observed kind (Stenflo 2009).

In the present paper we develop these ideas into a phenomenological extension of current scattering theory and use it to successfully model the observed  $D_1$  polarization in great quantitative detail. Through use of experimental data in the well-understood  $D_2$  line to constrain the values of the collisional and optical depth parameters  $\gamma_c$  and  $\tau$  it becomes possible to avoid the use of adjustable parameters when fitting the  $D_1$  data.

## 2. Laboratory experiment

After initial attempts failed to do the laboratory exploration of  $D_1$  scattering physics for the sodium  $D_1$  line with the use of a broad-band light

source, we realized that a tunable laser was required to achieve the needed S/N ratio with clean separation between the  $D_2$  and  $D_1$  transitions and insignificant stray light. In addition the tuning gives us the precise shapes of the polarization profiles.

We then chose to do the experiment for potassium instead, since solid-state tunable lasers are not available for the sodium wavelength range. The K I  $D_2$  7665 Å and the K I  $D_1$  7699 Å lines have the same quantum number structure as the Na I  $D_2$  5890 Å and the Na I  $D_1$  5896 Å lines, including nuclear spin and hyperfine structure, so it is the same physics that is being tested with potassium as for sodium.

The set-up has been described in detail by Thalmann et al. (2006, 2009) together with examples of the experimental results. Here we provide a summary of what is relevant for the understanding of the theoretical modeling of the data. The heart of the system is a cross-shaped glass cell that contains the potassium gas. The cell was tailor-made for our experiment by the late Alessandro Cacciani in Rome, who had perfected the art of building such cells for use in magneto-optical narrow-band filters used in helioseismology and solar magnetometry (Cacciani & Fofi 1978; Cacciani et al. 1997). Metallic potassium in the stem of the cell is heated to give potassium gas at a temperature of 100° C at the cell center, where the scattering takes place. An argon buffer gas is used to suppress diffusion of the potassium vapor towards the cooler entrance and exit windows, to avoid deposits that could make the windows opaque.

The spectral band width of the laser beam is not exactly known, but it is at least less than 2 mÅ. This is much smaller than the separation between the  $F = 1$  and  $F = 2$  hyperfine levels of the ground state, which is 9.1 mÅ, but it is comparable to the corresponding hyperfine splitting of the upper state of the K  $D_1$  line, which is 1.14 mÅ.

The expanded laser beam is passed through polarizers that allow us to select one of six states of 100% fractional polarizations in Stokes  $Q$ ,  $U$ , or  $V$  before the beam enters the cell: 100%  $\pm Q/I$ ,  $\pm U/I$ , or  $\pm V/I$ . Positive Stokes  $Q$  is defined to be linear polarization oriented perpendicular to the scattering plane. The scanning can be done with either of two separate laser heads, one for tuning around the K  $D_2$  resonance, the other for tuning

around the K  $D_1$  resonance.

In the output arm that receives light scattered by the cell at 90°, a piezoelastic modulator followed by a linear polarizer converts the polarization information (Stokes  $Q$ ,  $U$ , or  $V$ ) into intensity modulation, at 84 kHz for  $Q$  and  $U$ , at 42 kHz for  $V$ , while Stokes  $I$  is represented by the unmodulated (DC) signal. A photomultiplier feeds the signal to a lock-in amplifier, which demodulates the AC component. The combination of 6 alternative input states with three alternative output states for the polarization gives us 18 possible combinations. For each of them the laser tuning gives us the precise profile shape with mÅ resolution.

Furthermore a set of Helmholtz coils mounted on the cell allows us to impose on the cell center an external magnetic field with any strength in the range between  $\pm 30$  G, with an orientation that can be chosen to be in either of the three spatial directions: perpendicular to the scattering plane, parallel to the input beam, or parallel to the scattered beam.

Because the available parameter space of the experiment is so large, time and manpower only allowed the experiment to be carried out for some strategically selected combinations among the various possibilities. In the present paper we focus on the interpretation of the transverse field case (field perpendicular to the scattering plane) for the two combinations (1) Input 100%  $Q/I$  polarization, output detection of Stokes  $Q$ , and (2) input 100%  $V/I$  polarization, output detection of Stokes  $V$ . This selection was done not only because these cases were most thoroughly measured, but because conventional scattering theory predicts null results for case (1) and nearly null for case (2). This leads us to identify the observed polarization effects for these cases as due to previously overlooked, neglected physics.

### 3. Physics of polarized scattering

#### 3.1. Theoretical overview

Let us consider a scattering transition between the magnetic substates labeled  $a$  (initial state),  $b$  (intermediate), and  $f$  (final) and introduce the area-normalized complex profile function for ra-

diative absorption:

$$\Phi_{ba} = \frac{2/i}{\omega_{ba} - \omega - i\gamma/2}, \quad (1)$$

where

$$\omega_{ba} = (E_b - E_a)/\hbar \quad (2)$$

represents the transition frequency between the energy levels of the upper and lower magnetic substates, while  $\omega$  is the frequency of the incident radiation. Then the Kramers-Heisenberg formula for the probability amplitude for the scattering process  $a \rightarrow b \rightarrow f$  may be written as

$$w_{\alpha\beta} \sim \langle f | \hat{\mathbf{r}} \cdot \mathbf{e}_\alpha | b \rangle \langle b | \hat{\mathbf{r}} \cdot \mathbf{e}_\beta | a \rangle \Phi_{m\mu_a} \quad (3)$$

(cf. Stenflo 1994, 1998).

The matrix transition elements contain the scalar products between the dipole moment operator (proportional to the position vector  $\mathbf{r}$ ) and the unit vectors  $\mathbf{e}_\beta$  and  $\mathbf{e}_\alpha$  of the incident and scattered radiation field, respectively. Vector  $\mathbf{r}$  is decomposed in the three spherical vector components labeled by  $q = 0, \pm 1$ , which equal the difference  $\Delta m$  between the magnetic quantum numbers of the lower and upper states (with the quantization axis defined to be along the magnetic field vector), while the polarization components of the radiation field are real linear unit vectors that reside in the plane that is perpendicular to the propagation direction.

For classical scattering the probability amplitude is represented by the Jones matrix

$$w_{\alpha\beta} \sim \Phi_{-q} \varepsilon_q^{\alpha*} \varepsilon_q^\beta, \quad (4)$$

where the  $\varepsilon$  factors embody the scalar products between  $\mathbf{r}$  and  $\mathbf{e}_{\alpha,\beta}$  (cf. Stenflo 1994). With our definition of  $q$ , we have  $\Phi_{-q} = \Phi_{ba}$  for the case of a  $J = 0 \rightarrow 1$  absorption transition. In the general quantum-mechanical case we can write the Kramers-Heisenberg amplitude in the following analogous form, to bring out the similarities and differences with respect to the classical case as transparently as possible:

$$w_{\alpha\beta} \sim \Phi_{ba} \varepsilon_{q'}^{\alpha*} \varepsilon_q^\beta t_{fb} t_{ba}. \quad (5)$$

Here  $t_{ba}$  and  $t_{fb}$  represent the transition amplitudes for absorption and emission between the respective magnetic substates. They are all real

quantities, but their relative signs are of importance. All the other factors in Eq. (5) are in general complex-valued quantities.

Since the magnetic quantum numbers for the  $a$  and  $f$  states may differ, the corresponding  $q$  indices may also differ, which is the reason for using a prime for  $q$  in the case of the emission transition. In the classical case  $q' = q$ , and the three resonances (corresponding to the three  $q$ ) have equal probability amplitude and are driven in phase by the incident radiation field. In the quantum case the scattering amplitudes get weighted by the relative complex amplitudes  $c_a$  of the initial state  $a$ .

To go from the scattering probability amplitudes  $w_{\alpha\beta}$ , which represent the elements of a complex  $2 \times 2$  matrix  $\mathbf{w}$ , to obtain the scattering probabilities for the different polarization states, one forms the bilinear products  $w_{\alpha\beta} w_{\alpha'\beta'}^*$ , which are elements of a tensor product of type  $\mathbf{w} \otimes \mathbf{w}^*$  with appropriate summations over the various atomic states.

The standard approach in quantum scattering theory has been the ‘sum over histories’: To obtain the total probability amplitude for scattering from state  $a$  to state  $f$ , one sums over the probability amplitudes for all the possible intermediate states, while keeping the initial and final states  $a$  and  $f$  fixed. One then forms the bilinear product to obtain the probabilities, and afterwards sums over all the possible initial and final states  $a$  and  $f$ . This results in a complex  $4 \times 4$  coherency matrix  $\mathbf{W}$  of the form

$$\mathbf{W} = \sum_a |c_a|^2 \sum_f \left( \sum_b \mathbf{w} \right) \otimes \left( \sum_{b'} \mathbf{w}^* \right) \quad (6)$$

(Stenflo 1994, 1998).

There is a very fundamental distinction between the various summations here: While the sum over the intermediate states is *coherent* (done as a linear superposition of the probability amplitudes), the sums over the initial and final states are *incoherent* (done over the bilinear products that represent probabilities), weighted by the relative populations  $|c_a|^2$  of the initial states. The quantum interference phenomena are then exclusively due to the cross products that arise when the sums over  $b$  and  $b'$  are multiplied with each other.

In the present paper we will present experimental and theoretical evidence that demonstrates

that Eq. (6) with its separation between coherent and incoherent summations is incorrect, and that instead all summations should be done coherently (as previously suggested in Stenflo 2009). The correct expression should therefore be

$$\mathbf{W} = \left( \sum_{abf} c_a \mathbf{w} \right) \otimes \left( \sum_{a'b'f'} c_{a'}^* \mathbf{w}^* \right). \quad (7)$$

Note that it is absolutely essential to make the summation coherent not only over the initial states (accounting for the non-diagonal density matrix elements  $c_a c_{a'}^*$ ), but also use *coherent summation over the final states*. This rule is demanded both by a theoretical selection rule (cf. Sect. 3.4) and by the experimental data. If it is obeyed, then we can reproduce in great detail the results of the laboratory experiment, while if it is disobeyed we get zero polarization in the corresponding test cases. The selection rule in Sect. 3.4 implies that there is a strict coupling between the initial and final state coherences.

Since in this case each sum contains a much larger number of terms, the physical system will contain a much richer set of coherences and quantum interference phenomena, which are prevented in the earlier approach to quantum scattering as represented by Eq. (6). The new terms allow us to theoretically reproduce the results of our laboratory experiment in great quantitative detail in situations when the old formalism predicts zero polarization.

The practical implementation of the formally simple and symmetric Eq. (7) is however difficult, both conceptually and technically, since we need a way to determine the phase relations between the different ground level amplitudes  $c_a$ . In the absence of a radiation field the relative phases are random. In the presence of an incident radiation field the transverse oscillations of the electric vector drive the dipole resonators of the atomic system. It is this synchronized driving that produces phase locking between combinations of  $c_a$  level amplitudes. The heart of the problem is how to deal with this phase locking, which must be distinguished from conventional optical pumping, although it may superficially resemble it. To conceptually understand the fundamental distinction between phase locking and optical pumping we need a non-traditional way to look at the nature of quantum transitions, an issue that will be

addressed in the next subsection.

Before proceeding with the theoretical issues, let us already at this stage present experimental evidence that backs up our previous statements. In Fig. 1 we show the case of  $90^\circ$  scattering of K  $D_1$  radiation when the incident light is 100% linearly polarized perpendicular to the plane of scattering (incident Stokes  $Q/I = 1$ ), and we measure Stokes  $Q$  of the scattered radiation. The laser has been tuned across the  $D_1$  resonance, which gives us the profile shape. Standard scattering theory (Eq. (6)) predicts exactly zero  $Q$  polarization for all wavelengths, while with Eq. (7) we are able to reproduce the observations in great quantitative detail. Note that the observed  $Q$  is negative, i.e., the scattered radiation is weakly linearly polarized *parallel* to the scattering plane.

In the following sections we will explain what explicitly goes into these calculations, how the theory is extended to include the new physical effects, and how observations of the well-behaved  $D_2$  system are used to constrain the theory and enforce consistency. An objective is to provide convincing evidence that quantum scattering has a far richer coherency structure than allowed by the old formalism of Eq. (6), and to indicate the direction in which the theory should be extended to cover these phenomena.

To conclude this subsection we give the well-known expression for how to obtain the Mueller matrix  $\mathbf{M}$  that describes scattering of the Stokes vector from the complex coherency matrix  $\mathbf{W}$ :

$$\mathbf{M} = \mathbf{T} \mathbf{W} \mathbf{T}^{-1}. \quad (8)$$

The complex  $4 \times 4$  matrices  $\mathbf{T}$ ,  $\mathbf{T}^{-1}$  in Eq.(8) are purely mathematical transformation matrices without physical contents (cf. Stenflo 1994).

### 3.2. Wave packet interaction: Quantum blip or radiation bath?

An obstacle to a more complete understanding of the interaction of the atomic system with the radiation field has been the often prevailing misconception that atomic transitions are instantaneous events, quantum ‘blips’. To make our conceptual discussion of the interaction process as transparent as possible we will refrain from applying the second quantization formalism with the quantization of the electromagnetic field and instead use a semi-

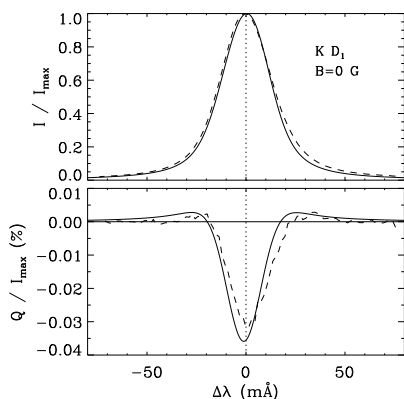


Fig. 1.— Polarized  $D_1$  scattering by potassium when the incident radiation is 100% linearly polarized perpendicular to the scattering plane ( $Q/I = 1$ ). The radiation scattered at  $90^\circ$  is then partially polarized *parallel* to the scattering plane (output  $Q$  negative). The observations (dashed curves) can be reproduced by the theory (solid curves) when the coherences in both the initial *and* final states are accounted for as in Eq. (7). If the coherences in the final state would be neglected, we would get zero polarization for all wavelengths, regardless of how unbalanced the  $m$  state populations are.

classical approach in which photons are treated as exponentially damped wave packets.

The misconception of instantaneous quantum jumps has been amplified by the circumstance that a theory for polarized optical pumping is only available under the assumption that the incident radiation is broadband in frequency (the flat-spectrum approximation, cf. p. 257 in Landi Degl’Innocenti & Landolfi 2004). Although the flat-spectrum assumption only requires the radiation to be spectrally flat over ranges comparable to the Doppler width of spectral lines, let us for conceptual clarity first consider the extreme case of complete flatness. With Heisenberg’s uncertainty principle  $\Delta E \Delta t \approx \hbar$  such a case implies that  $\Delta t = 0$ , i.e., the impinging wave packets have zero coherence length. Such wave packets do not exist in nature. Furthermore, this limitation contradicts the principle that each wave packet can be represented as a linear superposition of its monochromatic Fourier components.

While the flat-spectrum approximation does not imply this extreme case of zero coherence length, it does imply wave packets with a coherence length that is about two orders of magnitude smaller than actual wave packets, since the Doppler width is typically two orders of magnitude larger than the radiative damping width. For this reason the implications of this approximation are qualitatively of the kind indicated by our discussion of completely flat radiation. Thus, in terms of hypothetical (non-existing) broad-band wave packets the pumping scenario is a sequence of almost discrete pumping events, in which each quantum jump due to radiative excitation is nearly instantaneous. During the relatively long waiting times between each discrete event the atomic system is subject to the depolarization effects of collisions and magnetic fields (cf. the more extended discussion of this topic in Stenflo 2011).

It is only meaningful to talk about quantum ‘blips’ when a wave packet is recorded in a detector (collapse of the wave function). Before this happens the wave packets are not small entities but huge, with coherence lengths of several meters (in the absence of collisional effects). The radiative damping constant of potassium  $D_1$  and  $D_2$  is approximately  $\gamma = 3.8 \times 10^7 \text{ s}^{-1}$  (determined by the inverse life time of the excited state in the collisionless case), implying that the damped emission

process takes place over a time of order  $1/\gamma$ , which is  $10^7$  times longer than the time scale for the oscillation of the electric vector. During this long time light travels approximately 8 m, corresponding to  $10^7$  wavelengths.

With this enormous separation of time scales wave packets represent (from the point of view of the atomic system) a radiation bath. During the interaction with the atomic system the various dipole resonances in the atom are driven  $10^7$  times by the electric field of the single wave packet. This gives plenty of time to establish synchronization between the phases of the various dipole oscillators represented by the potential radiative transitions between lower and upper magnetic substates. In the case of the  $D_1$  atomic system there are 36 different allowed combinations of dipole transitions between lower and upper  $m$  states. Since all of them are subject to the driving force from the same external oscillating electric field (provided by a single incident wave packet), phase synchronizations will be established, depending on the polarization of the incident wave packet.

Both the lower and upper  $J = 1/2$  states of the  $D_1$  atomic system is split due to the nuclear spin into total angular momentum states  $F = 1$  (with three magnetic substates) and  $F = 2$  (with five magnetic substates). There are thus 8 magnetic substates in each of the lower and upper state. Various combinations of the 36 allowed dipole transitions have common  $m$  states (either lower or upper ones). For instance, a  $\Delta m = 0$  transition from upper state  $F = 1, m = 0$  couples to both  $F = 1, m = 0$  and  $F = 2, m = 0$  in the lower state. Since both the upwards and downwards transitions are jointly driven by the same oscillating electric field, phase synchronization between the two  $F = 1, m = 0$  and  $F = 2, m = 0$  lower states will be produced, which then leads to new polarization effects through Eq. (7).

Let us for completeness mention here that the fully quantized formulation of polarized scattering that was pioneered by Bommier (1997a,b) does not make use of the flat-spectrum approximation. Although the method is general with the potential of being extended to the multi-level case, it has so far only been implemented for the two-level case.

### 3.3. Coherences of the atomic system

We have in the previous subsection seen that the wave packet interaction is not associated with instantaneous quantum jumps, but that the atomic system with its various dipole resonators (36 in the  $D_1$  case) is immersed in a radiation bath (provided by each single wave packet), which drives the atomic oscillations and couples combinations of oscillators.

This viewpoint is largely prohibited when the flat-spectrum approximation is used, as indicated in the previous section. There are nevertheless good reasons why this approximation has represented the established approach, because by removing it we open a ‘Pandora’s box’ of coherency phenomena that we do not know how to properly deal with. However, by keeping the lid shut on this Pandora’s box we prevent access to the world of coherency phenomena in which a solution of the  $D_1$  enigma is to be found.

In the present paper we open the lid to examine the phenomena in this new world and try to show how they are responsible for the observed polarization features in the laboratory experiment. In view of the complexity of the interconnected coherences our initial approach has to be heuristic and phenomenological in nature rather than representing an attempt at a formulation of a new general theory. Still we go to great lengths to make the phenomenological extension of standard scattering theory well defined, internally consistent, based on the soundest possible arguments, and avoiding free parameters as far as possible. This effort is only possible with the guidance of experimental data. The success of our extension is that it is capable of modeling the key experimental data in great quantitative detail.

In the present subsection we will examine the nature of the various new coherences. For a conceptual understanding we begin by examining how phase synchronization or phase locking plays out in classical physics.

#### 3.3.1. Coherences in classical scattering

The equation for a classical oscillator in an external magnetic field can be written as

$$\frac{d^2 r_q}{dt^2} - (2qi\omega_L - \gamma) \frac{dr_q}{dt} + \omega_0^2 r_q = -\frac{e}{m} E_q \quad (9)$$

in component form, when instead of the three Cartesian spatial coordinates the three complex spherical vector components, labeled with  $q = 0, \pm 1$ , are used. The  $q = 0$  component is aligned along the magnetic field.  $r_q$  is the component of the position vector of the oscillator,  $\omega_L = eB/(2m)$  is the Larmor frequency.  $\gamma$  represents the damping due to the radiative energy loss of the oscillating system, and  $\omega_0$  is the resonance frequency of the system (cf. Stenflo 1994).

The advantage of using the complex spherical vectors rather than real linear vectors is that the component equations then decouple and represent three independent oscillators. Still, although the three equations are mathematically uncoupled (the equation system is diagonalized), the three oscillators are phase locked because the three components  $E_q$  of the driving oscillating electric field of the external radiation bath are mutually phase locked (since they are components of the same oscillating vector).

The solution of the stationary equation, when the oscillator is immersed in an eternal, monochromatic radiation bath, leads to the profile function  $\Phi_{-q}$ , which is proportional to the complex refractive index of the medium. As the dipole radiation emitted by these oscillators represents the scattered light, we readily obtain the Jones scattering matrix in the form of Eq. (4).

The frequency redistribution, i.e., the relation between the incident and scattered frequencies, can be obtained by solving Eq. (9) as a time-dependent problem (Bommier & Stenflo 1999). The full solution of this problem is the sum of the stationary solution and a transitory solution. The collisional effects are generally described in two ways: As phenomenologically introduced branching ratios between the stationary and transitory solutions, and as phase truncations of the oscillators, which lead to depolarization. Here we will not deal with the details of such redistribution effects, since they are not crucial for the key issues in the extension of scattering theory.

However, one aspect that is fundamental to this extension and which can be correctly described by the classical theory is the partial decoherence of jointly driven oscillators that have different resonant frequencies. In the absence of magnetic fields, the three classical oscillator components have the same resonant frequencies and therefore remain in

phase for the duration of the radiation bath, there is no decoherence. When however there is a frequency split induced by the Larmor frequency, the oscillators get progressively out of phase, depending on the ratio between the time scales of Larmor precession and radiative decay. This partial decoherence leads to the polarization effects in the scattered radiation that are covered by the term ‘Hanle effect’.

The partial decoherence between jointly driven resonators, i.e., between jointly driven atomic dipole transitions, is by no means limited to decoherence between the magnetically split transitions (Hanle effect), but applies to the relative phase relations and decoherence for any split but jointly driven transitions. An example is the dramatic polarization effects seen on the Sun due to scattering at the Ca II H and K line system (Stenflo 1980), two lines of the D<sub>1</sub> – D<sub>2</sub> type (although without hyperfine structure). In this particular case the line separation is due to the fine structure splitting (different  $J$  quantum numbers). In the potassium case that we are dealing with the splitting is due to hyperfine structure (different  $F$  quantum numbers), and for non-zero magnetic fields due to Zeeman splitting as well.

When forming the bilinear products  $w_{\alpha\beta} w_{\alpha'\beta'}^*$  between the elements of the Jones matrix for the scattering probability amplitudes we get interference terms, in which the partial decoherence is contained in the products  $\Phi_{ba}\Phi_{b'a'}^*$  between the profile factors. An elegant mathematical transformation is to convert such profile products into sums:

$$\Phi_{ba}\Phi_{b'a'}^* \sim \cos \alpha e^{i\alpha} \frac{1}{2} (\Phi_{ba} + \Phi_{b'a'}^*) \quad (10)$$

(Stenflo 1994, 1998), where the angle  $\alpha$  is given by

$$\tan \alpha = \frac{\omega_{ba} - \omega_{b'a'}}{\gamma}. \quad (11)$$

In the case of magnetically induced splitting  $\alpha$  is referred to as the ‘Hanle angle’. The expression is however quite general and is valid regardless of the physical origin of the splitting.

With the conversion of Eq. (10) the interference effects due to the profile product gets factorized into a frequency-independent Hanle part  $\cos \alpha e^{i\alpha}$  and a frequency-dependent part, which becomes unity if we integrate over all frequencies



(since each profile function is area normalized). The Hanle part consists of an amplitude factor, which in the scattering polarization corresponds to depolarization, and a phase factor that corresponds to rotation of the plane of polarization.

The classical oscillator case corresponds to the quantum-mechanical case for a  $J = 0 \rightarrow 1 \rightarrow 0$  scattering transition. It also consists of three resonators, which link the three  $m$  state of the upper level to the common, single lower state. In such a situation  $a' = a$ , so there can be no lower-level coherences. In the general case when there are more than one lower state, ground-state coherences are possible, but since the coherency terms not only contain the profile products of Eq. (10) but also the level amplitude products  $c_a c_{a'}^*$ , these coherences will only play a role if there are correlations between the phases of certain combinations of level amplitudes. In the absence of an external radiation field the phases are uncorrelated, because there is no coupling between the levels. Remaining lower-level coherences will be erased if the time between collisions is much shorter than the ‘waiting time’ between successive radiative excitations. The needed synchronization between the phases can however be provided by the oscillating electric field of the wave packet radiation bath, which is a source of coupling or phase locking between combinations of ground states.

### 3.3.2. Coherences in the initial and final states

The coherences in the initial state are represented by the off-diagonal elements  $c_a c_{a'}^*$  of the density matrix. In the absence of outside disturbances (external radiation field or collisions), each level amplitude oscillates like  $\exp(-iE_a t/\hbar)$ . If the energy levels  $E_a$  and  $E_{a'}$  are not identical, the oscillations will rapidly get out of phase. Let us now assume that the phases get synchronized by the driving oscillating electric field of an incident wave packet, but that the initial phase synchronization decays with the damping rate  $\gamma$  because the driving electromagnetic wave packet is exponentially damped according to this rate. In the time domain the density matrix element is then  $\exp(-i\omega_{aa'} t - \gamma t)$ . The time derivative of this expression must for stationarity be balanced by the radiative absorption and emission rates, which represent the interaction between the driving oscillating electric field and the atomic system.

The balance equation then gives us the expression  $1/(i\omega_{aa'} + \gamma)$  for the corresponding density matrix element, which may more elegantly be written as

$$c_a c_{a'}^* \sim \frac{1}{1 + i \tan \beta} = \cos \beta e^{-i\beta} \quad (12)$$

(cf. Eq. (8.89) in Stenflo 1994). The angle  $\beta$  is given by

$$\tan \beta = \frac{\omega_{aa'}}{\gamma}. \quad (13)$$

Comparison with Eqs. (10) and (11) shows that this initial-state coherence is of the same general form as ‘Hanle type’ coherences between resonant transitions.

If the oscillating electric field of the incident radiation has a polarization that leads to radiative coupling between the  $a$  and  $a'$  states (via appropriate excited states), then we expect the constant of proportionality in Eq. (12) to be close to  $|c_a| |c_{a'}|$  (the product between the square roots of the sublevel populations), since when the phases of the level amplitudes are synchronized in the radiation bath, the only source of decoherence is the difference in oscillation frequency as expressed by the Hanle-type factor in Eq. (12). In the absence of any radiative coupling the proportionality constant would be zero, with the consequence that the respective initial-state coherence does not contribute to the scattering process. In the next subsection (Sect. 3.3.3) we will discuss the nature of this radiative coupling in some more detail using our laboratory experiment for potassium  $D_1 - D_2$  as an example.

As the energy separation between the  $a$  and  $a'$  levels increases, the initial-state coherence terms get suppressed towards zero by a ‘depolarization factor’  $\cos^2 \beta$  represented by the real part of the Eq. (12) expression. Because of the symmetry between the radiative excitation and deexcitation process, we expect there to be a similar suppression factor governing the final-state coherences. There is however a difference between the two legs of the  $a \rightarrow b \rightarrow f$  scattering process: the  $a \rightarrow b$  leg is associated with the complex  $\Phi_{ba}$  profile function of Eq. (1) while the  $b \rightarrow f$  leg is not. The imaginary part of Eq. (12) with its associated minus sign is related to the role of the complex profile function in the oscillation between the  $a$  and  $b$  states, which establishes the radiative coupling. No such complex-valued term is involved in the  $b \rightarrow f$  leg

(since the transition amplitudes  $t_{fb}$  are real numbers). Therefore it is most reasonable to expect that the final-state coherences should be governed by the symmetric version of Eq. (12), namely the sum of this expression with its complex conjugate (normalized to unity for zero splitting). This normalized sum equals the  $\cos^2 \beta$  suppression factor, with the difference that now  $\beta$  is not given by Eq. (13), but by the same equation if we replace  $\omega_{aa'}$  by  $\omega_{ff'}$ .

The only valid benchmark that we can use to test the validity of these rather heuristic arguments is experimental data. Fortunately the scattering polarization turns out to be extremely sensitive to the choices we make for the ground-state coherences. If we omit them, we get zero polarization, regardless of the relative initial  $m$  state populations. If we use Eq. (12) but set the final-state coherences to be unity (no suppression factor), we get much too large polarization effects. If we keep an imaginary part of the final-state coherences like for the initial state, then we also cannot achieve a fit with the data. The same happens if we omit the imaginary term in Eq. (12) or change its sign. Also we must only use the correct combinations of radiative couplings (cf. Sect. 3.3.3), otherwise we get results that have no resemblance with the observations. Only with the previously described choices of expressions for the coherence terms we succeed in obtaining a fit at all, and on top of that, the fit agrees with the observational data in great quantitative detail in a way that is consistent between  $D_1$  and  $D_2$  and between the Stokes  $I$ ,  $Q$ , and  $V$  parameters, including their profile shapes.

Let us note here that for a given initial-state ( $a, a'$ ) combination only certain ( $f, f'$ ) combinations for the final-state coherences are allowed. The nature of these selection rules will be addressed in Sect. 3.4. Without them we find no agreement with the observational data.

### 3.3.3. Radiative coupling in the $D_1 - D_2$ experiment

Our analysis here of the laboratory scattering experiment will focus on the cases when (1) the incident radiation is 100% linearly polarized perpendicular to the scattering plane, while the Stokes  $I$  and  $Q$  parameters of the  $90^\circ$  scattered radiation are recorded, and (2) when the incident radiation is 100% circularly polarized, while the Stokes  $I$

and  $V$  parameters of the scattered radiation are recorded. The imposed external magnetic field is chosen to be vertical (perpendicular to the scattering plane). This direction represents the quantization direction in our theoretical discussion.

Let us first turn our attention to case (1). Then among all the 36 resonators in the  $D_1$  system only those with  $m_a - m_b = q = 0$  get driven by the oscillations of the electric field of the incident wave packet, with the consequence that there can only be radiative coupling between initial  $a$  and  $a'$  states for which the  $m$  quantum number is identical ( $m_{a'} = m_a$ ). The only possibility for two such states to represent separate states is to belong to different  $F$  states.

Let us as a concrete example see how the two states ( $F = 1, m = -1$ ) and ( $F = 2, m = -1$ ) are radiatively coupled. Each of them couple by radiative excitation to each of the two corresponding states of the upper level. Similarly each of the two upper states are coupled to the corresponding two lower states by the emission process. The oscillating electric field drives the upwards and downwards oscillating transitions with equal transition strength.

All the four  $m = -1$  states (two lower and two upper) are therefore mutually phase locked as a consequence of the common driving external electric field. For the same reason that we have phase synchronization between the three classical oscillators (which leads to the Hanle factor of Eq. (10) for the upper states of a  $J = 0 \rightarrow 1$  transition), the oscillatory symmetry between the upper and lower states imply the presence of a corresponding phase synchronization between pairs of ( $a, a'$ ) states with the Hanle type factor of Eq. (12).

For our case (1) we therefore set the proportionality constant in Eq. (12) to its maximum value that represents full phase synchronization whenever  $m_{a'} = m_a$ , zero otherwise. This choice brings excellent agreement between theory and observations, as illustrated in Figs. 1 and 3. If we would set the proportionality constant to its maximum value for all ( $a, a'$ ) combinations we would get large positive  $Q$  polarization, in contradiction with the laboratory experiment, while omitting the ground-state coherences leads to exactly zero for all wavelengths in Fig. 1.

Now let us consider our case (2), when the in-

cident radiation is 100% circularly polarized and the magnetic field is transverse. In this case the electric field of the incident wave packets oscillates with equal amplitudes parallel and perpendicular to the magnetic field, which means that both the  $q = 0$  and  $q = \pm 1$  resonators of the atomic system are excited. This leads to radiative coupling between *all* the resonators and therefore between all the  $(a, a')$  combinations. Consequently we should set the constant of proportionality in Eq. (12) to its maximum value for all these combinations. Doing this we indeed get excellent agreement between theory and experimental data, as illustrated in Fig. 4, while other choices do not lead to comparable success. If we remove all ground-state coherences, we get an order of magnitude too small polarization. This residual polarization is exclusively due to quantum interferences in the excited state.

### 3.4. Phase closure as selection rule

The ground-state coherences that govern the polarization of the scattered radiation via Eq. (7) have contributions from both the initial and final states. In the previous section we have indicated how the initial-state coherences are determined by the radiative coupling between the initial  $m$  states. In the present subsection we will show that all final-state interferences are not allowed but that they are governed by selection rules that couple them to certain combinations of initial-state coherences. Therefore an initial-state coherence will only contribute to the polarization of the scattered radiation if it is coupled in the scattering process to a final-state coherence in a way that obeys the selection rule.

The selection rule that governs which combinations of initial and final  $m$  states are allowed can be formulated as a requirement of *phase closure*, a concept that was introduced in Stenflo (2009). It has its origin in the geometrical  $\varepsilon$  factors in Eq. (5), which represent the scalar product between the transverse radiation-field basis vectors  $\mathbf{e}_{\alpha, \beta}$  and the complex spherical basis vectors  $\mathbf{e}_q$  (with  $q = 0, \pm 1$ ) of the atomic system.

The basis vectors  $\mathbf{e}_q$  are defined such that  $\mathbf{e}_0$  is along the magnetic field or quantization axis. In this coordinate system the scattering geometry is specified by colatitude  $\theta$  and azimuth  $\phi$ , defined with respect to some arbitrarily chosen zero point.

The scattering geometry of our laboratory experiment is such that  $\theta = 90^\circ$  for both the incident and scattered beam, while the scattering angle is given by  $\phi' - \phi$ , the azimuth difference between the scattered and incident radiation. All the azimuth dependence is contained in  $\varepsilon_{\pm}^{\alpha}$  and  $\varepsilon_{\pm}^{\beta}$  in the form of a phase factor  $\exp(\pm i\phi')$  or  $\exp(\pm i\phi)$ , regardless of the values of  $\alpha$  and  $\beta$  (cf. Eq. (3.86) in Stenflo 1994). The complex value of this phase factor depends on the arbitrary choice of zero point for the azimuths in the coordinate system used.

It would be unphysical if the polarization of the scattered radiation would in any way depend on this choice of coordinate system. Therefore only combinations of  $\varepsilon$  factors for which the choice of zero point cancels out can represent physical scattering processes. This gives us a selection rule that we refer to as the requirement of phase closure. The zero point of the azimuth scale cancels out if all the physical effects depend exclusively on the *difference*  $\phi' - \phi$  between the scattered and incident azimuth directions, but never on the absolute value of either azimuth.

Each term in the Mueller scattering matrix is made up of the bilinear products between scattering amplitudes because of the tensor product in Eq. (7). Since each scattering amplitude contains two  $\varepsilon$  factors, since  $\varepsilon_q^{\beta*} = -\varepsilon_{-q}^{\beta}$  when  $q = \pm 1$ , and since  $q$  represents the difference between the lower and upper  $m$  quantum numbers of the transition, each Mueller matrix element contains four  $\varepsilon$  factors of the type

$$\varepsilon_{m_a - m_b}^{\beta} \varepsilon_{m_b - m_f}^{\alpha} \varepsilon_{m_{f'} - m_{b'}}^{\alpha} \varepsilon_{m_{b'} - m_{a'}}^{\beta}. \quad (14)$$

$\varepsilon$  factors relating to the  $a \rightarrow b$  transition contain the azimuth  $\phi$  for the incident radiation, while  $\varepsilon$  factors relating to the  $b \rightarrow f$  transition contain the azimuth  $\phi'$  for the scattered radiation. If the combined complex phase factor for our product of four  $\varepsilon$  factors is  $\exp(i\delta)$ , then we see from Eq. (14) that

$$\begin{aligned} \delta = & (m_a - m_b) \phi + (m_b - m_f) \phi' \\ & + (m_{f'} - m_{b'}) \phi' + (m_{b'} - m_{a'}) \phi. \end{aligned} \quad (15)$$

If we would change the zero point and replace  $\phi$  and  $\phi'$  with  $\phi - \phi_0$  and  $\phi' - \phi_0$ , we see that the dependence of the phase on  $\phi_0$  only disappears if the factor in front of  $\phi$  equals the negative of the

factor in front of  $\phi'$ . This gives us the selection rule

$$m_f - m_{f'} = m_a - m_{a'}. \quad (16)$$

This phase closure relation thus demands that only the final-state coherences that have the same  $\Delta m$  as the initial-state coherences are allowed. Note that the magnetic quantum numbers of the excited state are not involved at all, the rule only dictates how the initial and final state coherences are coupled.

In our efforts to reproduce the observational data we discovered an additional selection rule that seems to govern the coupling between the initial and final state coherences:

$$F_f - F_{f'} = F_a - F_{a'}. \quad (17)$$

It was not anticipated and only found by trial and error: With it we got excellent fits to the observational data, without it the disagreement with the data was very large. With afterthought Eq. (17) is sensible, since then the scattering transition radiatively couples only coherences that oscillate in the same sense. A coherence between  $F = 1$  and 2, for instance, oscillates like  $\exp[-i(E_1 - E_2)t/\hbar]$ . A coherence with the reversed order of the states would oscillate in anti-phase. Symmetry of the scattering process seems to demand that couplings with anti-phase oscillations are prohibited. At present we lack a full understanding of this rule, but it is empirically required to get agreement with the observations.

#### 4. Theoretical modeling of the experimental data

Although the calculation of scattering amplitudes from Eq. (5) is well-known and uncontroversial, it is technically difficult for our  $D_1 - D_2$  case, because we have hyperfine structure splitting and are in the Paschen-Back regime, in which the Zeeman splittings and the transition amplitudes vary with field strength in a non-linear way. In support of the present project S.V. Berdyugina and D.M. Fluri (priv. comm.) kindly provided us with an IDL routine that they had written, which calculates the set of transition amplitudes, resonance wavelengths, and energy levels for any given field strength in the case of the potassium or sodium  $D_1$  or  $D_2$  system. The correctness of the program has been tested through comparison with other codes

as part of the work of Sowmya et al. (2014). With this program the calculation of scattering amplitudes according to Eq. (5) becomes a straightforward task.

When trying to theoretically reproduce the observational data from our laboratory experiment there are three other effects to be considered, which we have not discussed so far: (1) Effects of collisions on the scattering polarization (will be dealt with in Sect. 4.1). (2) Optical depth effects with magnetically induced dichroism (will be dealt with in Sect. 4.2). (3) Optical pumping of the lower  $m$  state populations.

While (1) and (2) will be accounted for, we choose to leave (3) aside in our modeling presentation here. The reason is that optical pumping that creates unbalanced  $m$  state populations only modifies the results quantitatively by modest amounts, not qualitatively, in contrast to the fundamental issues that we have addressed in the previous sections concerning the treatment of the initial and final state coherences and the selection rules, all of which have dramatic effects on the modeling. Since the ‘waiting time’ between successive radiative absorption events is in general much longer than the time between collisions with the argon buffer gas, much of the population imbalances can be expected to be erased before each scattering event.

We nevertheless did modeling experiments also with inclusion of optical pumping that gives us the populations  $|c_a|^2$ , but even when the effects of collisions were entirely disregarded in the pumping problem the effects on the scattering polarization were not dramatic. It was easier to find a good fit to the observations when such pumping was not included. Pumping does not play an essential role in the context of identifying the missing physics in polarized scattering. Including it introduces new free parameters because the effect of collisions on the pumping process, which certainly plays a significant role, is not sufficiently known. For such reasons attempts to properly deal with optical pumping would distract from the main issues of the paper and not lead to improved fits of the data.

#### 4.1. Effects of collisions

The vapor cell used for our scattering experiment is small and very convenient to handle. A heating coil in the stem of the cell vaporizes the metallic potassium to produce the gas in the cell center at which the scattering takes place. With a gas temperature of 100° C we get high enough number density of potassium atoms to provide the scattered light needed to measure small degrees of polarization.

To suppress diffusion of the potassium gas, which could lead to deposits on the cooler entrance and exit windows and make them opaque, an argon buffer gas is used in the cell. Unfortunately this has the disadvantage that the potassium atoms are subject to a high collision rate, which affects the scattering polarization in significant ways.

The collisions cause line broadening by changing the effective damping constant of the profile functions, as well as depolarization of the emitted radiation. Let us, as is customary, denote the collisional damping constant by  $\gamma_c$ , while the natural, radiative damping constant is  $\gamma_N$ . Then the effective  $\gamma$  that governs the line shape in Eq. (1) is  $\gamma_N + \gamma_c$ .

The collisional depolarization effects, which destroy the phase relations in the scattering process to make the scattered light unpolarized and isotropic can be expressed in terms of the depolarization factor

$$k_c = \frac{\gamma_N}{\gamma_N + D^{(K)}}, \quad (18)$$

where  $D^{(K)}$  with  $K = 1$  or  $2$  represents the destruction rates of the  $2K$  multipoles of the atomic system. In time-dependent classical scattering theory (Bommier & Stenflo 1999)

$$D^{(K)} = 0.5\gamma_c \quad (19)$$

for both  $K = 1$  (atomic orientation) and  $K = 2$  (atomic alignment). In the classical theory the collisions truncate the exponentially damped atomic oscillations. After Fourier transformation we then get the factor of 0.5 in Eq. (19). In detailed quantum mechanical calculations of the scattering process the resulting value for this factor depends on the atomic system but stays typically within at least a factor of two around the classical value. In

the absence of other data our best choice is therefore to use the relation represented by Eq. (19).

The depolarization factor  $k_c$  is used to scale all elements of the Mueller scattering matrix except the first one ( $M_{11}$ ), which represents isotropic scattering. This is a simplified treatment, but in view of the large collisional rates and the use of these rates for a parametrization of the problem, it is not justified here to go into the intricacies of partial frequency redistribution theory.

The suppression effect from the depolarization caused by  $k_c$  is largely compensated for by the increased overlap and interference between the ground-state sublevels due to the collisional broadening, as described by Eq. (13). The question is however what collision-modified expression for  $\gamma$  we should use in Eq. (13), e.g.  $\gamma_N + \gamma_c$  or  $\gamma_N + D^{(K)}$ ? On the one hand one may argue for the first of these two choices, since these coherences are determined by the radiative couplings between the various combinations of allowed transitions, and these couplings are governed by the profile functions in which  $\gamma = \gamma_N + \gamma_c$ . On the other hand there is a good case for the second expression, since the depolarization factor used for the upper-state coherences is based on  $D^{(K)}$ . Through experimentation with both versions we find that the best fit results are obtained if we use an average between the two cases. This implies that we for the effective  $\gamma$  in Eq. (13) use  $\gamma_N + 0.75\gamma_c$ . For symmetry reasons we use the same expression for the initial and final state coherences.

Let us stress that the choice of the expression for  $\gamma$  to be used for the ground-state coherences is not crucial for our investigation. It does not lead to any qualitative changes, but only affects the quantitative details of the model fitting. Our aim here is to make the choices that appear most reasonable while minimizing the number of free parameters.

If we thus fix the choices for the three relations used to describe the effects of collisions,  $\gamma_N + \gamma_c$  to describe the shape of the profile function,  $\gamma_N + 0.5\gamma_c$  to describe the collisional depolarization factor used for the Mueller matrix elements, and  $\gamma_N + 0.75\gamma_c$  to describe the effect on the ground-state coherences, then we are left with a single free collisional parameter, namely  $\gamma_c$ .

## 4.2. Optical depth effects

The optical depth of the potassium gas must be non-zero, otherwise we would not get any scattered photons. Choosing the working temperature of the cell represents a compromise: we want to optimize the number of scattered photons to get a good signal, while avoiding multiple scattering or excessive optical depth effects. The finite optical depth leads to enhanced absorption at line center, which may change the profile shape, and also causes dichroism when a magnetic field is present. Comparison between our theory and the experimental data shows that the optical depth effects are too small for significant multiple scattering, but large enough to cause significant line broadening and magnetically induced dichroism. They therefore need to be accounted for, but a single free parameter, the optical depth  $\tau$  at line center (where the optical depth reaches its maximum value) is sufficient. We find that the optimum fit value for  $\tau$  is 0.25 in the case of  $D_1$ , while it is twice this value for  $D_2$  because of its twice higher oscillator strength.

Our scattering experiment can be described as a transformation of the input Stokes vector  $\mathbf{S}_{\text{in}}$  into the output Stokes vector  $\mathbf{S}_{\text{out}}$  through

$$\mathbf{S}_{\text{out}} = \mathbf{M}_{\text{eff}} \mathbf{S}_{\text{in}}, \quad (20)$$

where  $\mathbf{M}_{\text{eff}}$  is the effective Mueller matrix of the system. When optical depth effects are accounted for, it can be represented by

$$\mathbf{M}_{\text{eff}} = \mathbf{M}_{\text{arm}} \mathbf{M}_{\text{scat}} \mathbf{M}_{\text{arm}}, \quad (21)$$

where  $\mathbf{M}_{\text{scat}}$  is the scattering Mueller matrix, the same as the  $\mathbf{M}$  that is given by Eq. (8), while  $\mathbf{M}_{\text{arm}}$  represents the Mueller matrix for the medium in an arm of the cell. There are two relevant arms here: The incident light goes through the input cell arm before it reaches the cell center, where it is scattered and then traverses the output cell arm before being analyzed for its polarization state and being detected. The Mueller matrices for the input and output arms are the same and surround the scattering matrix.

In the unpolarized case with an optical depth  $\tau$  at line center and an absorption profile  $\phi$  that is normalized to unity at line center, the effect of the medium would be absorption by the factor  $\exp(-\phi\tau)$  (since the contributions from emission

through scattering in the pencil-shaped geometry of the medium would give a negligible contribution in the particular beam direction in comparison with the absorption effects in that direction). In the polarized case, when the medium in a cell arm is described by the  $4 \times 4$  Mueller matrix  $\Phi$  instead of by a scalar absorption coefficient, the dichroic effects of the medium are represented by

$$\mathbf{M}_{\text{arm}} = e^{-\Phi \tau}. \quad (22)$$

The exponentiation of a matrix is defined by its Taylor expansion.

In a magnetized medium

$$\Phi = \begin{pmatrix} \phi_I & \phi_Q & \phi_U & \phi_V \\ \phi_Q & \phi_I & \psi_V & -\psi_U \\ \phi_U & -\psi_V & \phi_I & \psi_Q \\ \phi_V & \psi_U & -\psi_Q & \phi_I \end{pmatrix}, \quad (23)$$

where  $\phi_{Q,U}$  describe the transverse Zeeman effect,  $\phi_V$  the longitudinal Zeeman effect, and  $\psi_{Q,U,V}$  the magneto-optical effects, while  $\phi_I$  represents the effect of the Zeeman splitting on the intensity absorption profile (cf. Eqs. (6.58) and (6.59) in Stenflo 1994).

Since we are dealing with a very weakly magnetized medium (all field strengths that we consider here are below 20 G), all off-diagonal elements of  $\Phi$  are small in comparison with  $\phi_I$ . In our power series expansion of  $\exp(-\Phi \tau)$  we therefore only need to retain the terms of first order in these elements, while allowing the optical depth  $\tau$  to be of any higher order.

Here we will only model the case when the incident radiation is propagating perpendicular to the magnetic field direction, which also defines the positive Stokes  $Q$  direction. Then all dichroic elements of  $\Phi$  are zero except  $\phi_I$  and  $\phi_Q$ . In the case of circularly polarized light  $\phi_Q$  plays no role, the whole effect is in the form  $\exp(-\phi_I \tau)$ . However, in the case of linear  $Q$  polarization,  $\phi_Q$  is significant and represents the effects of magnetically induced dichroism.

Without this dichroism we are unable to explain the observed dependence of the scattered  $Q$  polarization on field strength, since our scattering theory alone does not predict any significant effect, even when the ground-state coherences are included. Comparison with our data gives us an

estimate of the value of  $\tau$  that is needed to explain the observed field dependence. Another constraint comes from the observed profile shapes. The line width increases with increasing  $\tau$ . It turns out that the value of  $\tau$  that gives us the right field dependence automatically also gives us the right line width.

For the calculation of the  $\Phi$  matrix we have to sum over the contributions from the various  $\phi_q$  profile functions ( $q = 0, \pm 1$ ) weighted by the corresponding transition strengths  $t_{ab}^2$ , to arrive at the expressions for  $\phi_I$  and  $\phi_Q$ . In this case the profile functions  $\phi_q$  are described by Voigt functions, having a Doppler width given by the thermal width at 100° C (10.2 mÅ) and a damping constant given by  $\gamma_N + \gamma_c$ , which is the same damping rate that governs the profile functions of the scattering process.

### 4.3. Using D<sub>2</sub> to determine the free parameters

With our previous definitions we are left with only two free model parameters,  $\gamma_c$ , which governs all the collisional effects, and  $\tau$ , which governs the dichroic or optical-depth effects. For physical consistency we further have the constraint that the same parameter values must be used for *both* the D<sub>1</sub> and D<sub>2</sub> observations. We are not allowed to use independent fit parameters for these two lines, since the same vapor cell is used for both. The only modification is that we need to use  $2\tau$  for D<sub>2</sub>, since it has twice as large oscillator strength and therefore twice as large optical thickness.

The ground-state coherence effects that we have been discussing play no significant role for the D<sub>2</sub> line, because D<sub>2</sub> has intrinsic polarization (from the upper level) that is larger by approximately a factor of 50 and therefore masks the ground-state effects. For this reason the D<sub>2</sub> line can perfectly well be described by standard scattering theory. By using the D<sub>2</sub> line to fix the values of our two free parameters, the obtained values become independent of the way in which we are dealing with the ground-state coherences. No further parameter fitting is then needed when addressing the D<sub>1</sub> problem.

Figure 2 shows the excellent fit we get to the observed Stokes *I* and *Q* D<sub>2</sub> profiles for the non-magnetic case when the incident radiation is 100 %

linearly polarized perpendicular to the scattering plane (*Q* type polarization). The dashed curves represent the observations, the solid curves the theoretical model with  $\gamma_c = 90 \gamma_N \approx 3.5 \times 10^9 \text{ s}^{-1}$  and  $\tau = 0.25$  (implying that the maximum optical depth at the D<sub>2</sub> line center is 0.50). The theoretical profiles have been convolved with a Gaussian having a Doppler width that equals the thermal width for 100° C. No additional instrumental broadening has been applied (we have no reason to expect any significant spectral smearing of the laser beam).

The fit in Fig. 2 is nearly perfect, except that there are some deviations in the distant wings of the *I* profile. The *Q* polarization amplitude scales directly with the depolarization factor  $k_c$ , which therefore gets fixed precisely by the data. Through Eqs. (18) and (19) this determines the value of  $\gamma_c$ .

The line width scales with  $\gamma_c$ , but it also increases with increasing  $\tau$ , since the absorption mainly suppresses the line core while having little effect on the wings. If we use the  $\gamma_c$  that is fixed by the *Q* amplitude but set  $\tau = 0$ , then the theoretical profiles are significantly narrower than the observed ones, and there would be a need for additional line broadening (e.g. due to some hypothetical instrumental smearing) to get agreement between the profile shapes. With our chosen value for  $\tau$  we get an excellent profile fit without the need for any such additional ad hoc broadening.

As we will see in the next subsection, the  $\tau$  that is needed to fit the D<sub>2</sub> profile shape is also the  $\tau$  that is needed to account for the field strength dependence of the D<sub>1</sub> *Q* polarization. It is gratifying to note that there is such consistency between the independent D<sub>2</sub> and D<sub>1</sub> constraints on  $\tau$ .

If we would increase the value of  $\tau$  significantly further, so that  $2\tau$  would start to become comparable to unity, then the D<sub>2</sub> Stokes *I* profile not only broadens but gets deformed by becoming double-humped with a depression at line center. The absence of any sign of such a deformation shows that we can safely rule out the possibility that the optical depth could be much larger than our present estimates. This conclusion refers only to the qualitative profile shape without using numerical values of any amplitudes or widths.

#### 4.4. Role of magnetically induced dichroism

In Fig. 1 we showed the results for  $D_1$  scattering in the non-magnetic case with the same geometry and same parameter values as for the  $D_2$  plot in Fig. 2. We note that the  $D_1$  polarization is of opposite sign and with about 50 times smaller amplitude than that of  $D_2$ . The laboratory experiment has the sensitivity to measure polarization effects down in the  $10^{-5}$  range. Such a sensitivity is needed to uncover the tiny polarization effects and profile shapes for  $D_1$  scattering. The access to this parameter range allows us to explore scattering physics in previously untested domains.

When for  $D_1$  doing the Stokes  $Q$  scattering for a sequence of different field strengths (with the field oriented perpendicular to the scattering plane) the laboratory experiment reveals a significant field dependence that scales with the square of the field strength. In contrast, a significant field dependence (within the studied field strength range) is absent in the computed  $Q$  polarization when the effects of the surrounding medium are not accounted for. If we however introduce a finite optical depth, then we get a field dependence that also scales with the square of the field strength, as it should when it is due to the transverse Zeeman effect. The amplitude of this dependence scales with  $\tau$ . Choosing  $\tau = 0.25$  gives good agreement with the observational data, as illustrated by Fig. 3.

The main source of this field dependence comes from the  $\phi_Q$  element of the dichroic  $\Phi$  matrix of Eq. (23), which represents the transverse Zeeman effect. In absorption the contribution from the  $\pi$  component in the line core is negative, while the  $\sigma$  contributions in the wings are positive, but in the  $\phi_Q$  profile they are balanced to make the integrated profile zero. However, the dichroic contribution to the  $Q$  polarization comes not from  $\phi_Q$  alone, but from its product with the intensity profile. This gives much more weight to the negative contribution from the line core than to the wing contributions. Therefore the net contribution is negative, with the consequence that the already negative non-magnetic scattering  $Q$  polarization gets enhanced.

Figure 3 shows the  $I$  and  $Q$  profiles for the largest field strength used in our laboratory experiment, 18.7 G. As in Fig. 1 the observations

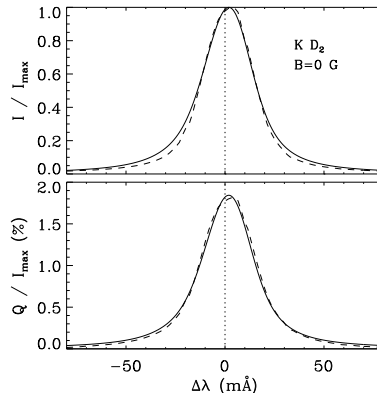


Fig. 2.— Stokes  $I$  and  $Q$  profiles for potassium  $D_2$  in the non-magnetic case when the incident radiation is 100% linearly polarized in the  $Q$  direction (perpendicular to the scattering plane) like in Fig. 1 that represented the  $D_1$  case. The same values for the free parameters,  $\gamma_c = 90\gamma_N$  and  $\tau = 0.25$ , are used for both the  $D_2$  and  $D_1$  cases. Note that the  $D_2$  polarization is about 50 times larger than the  $D_1$  polarization and of opposite sign.

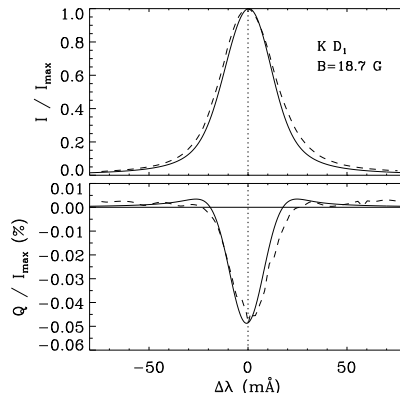


Fig. 3.— Stokes  $I$  and  $Q$  profiles for K  $D_1$  for the same geometry and parameters as in Fig. 1, except that here we show the case when the vertical magnetic field is 18.7 G (while it was zero in Fig. 1). Dashed curves: observations; solid curves: theory. The difference in polarization scale with respect to Fig. 1 is due to magnetically induced dichroism in the potassium gas. The systematic wavelength shift of the dashed  $Q$  curve relative to the solid one can be understood in terms of the time constant used for the lock-in amplifier to optimize the polarimetric sensitivity.



are represented by the dashed curves, the theory by the solid curves. The geometry and other parameters are the same as for Fig. 1, the only difference being the field strength. We see that an excellent fit is obtained, which would not have been the case without introducing the finite optical depth  $\tau = 0.25$ . Comparison between Figs. 3 and 1 shows that the profile shapes are almost unaffected by the magnetic field, but the polarization scales in the two figures are significantly different (although the difference is rather modest).

Both Figs. 3 and 1 give the (false) impression that the theoretical model is unable to reproduce the exact wavelength position of the  $Q$  profiles. The observational (dashed) curves for the  $Q$  profiles are seen to be systematically shifted towards the right relative to the theoretical (solid) curves. The magnitude of the shift is about  $2.8 \text{ m\AA}$ , which corresponds to about 1.7 step sizes in the stepwise wavelength tuning of the laser to scan the line profile.

The probable origin of this shift has to do with the time constant used by the lock-in amplifier when demodulating the polarization information, which for Stokes  $Q$  is at 84 kHz due to the piezoelectric modulation. To achieve polarimetric sensitivity down into the  $10^{-5}$  range one needs maximum temporal integration of the demodulated AC signal before it is read out. The chosen analog integration time should however be compatible with the scan rate. If the integration time is longer than the time between tuning steps, there will be a delay and overlap between the steps, resulting in shift and broadening of the demodulated profile. As such an analog time constant is not applied to the DC (Stokes  $I$ ) signal, the  $Q$  profile will be shifted (and slightly broadened) in the tuning direction with respect to the  $I$  profile. The observed shift that is of order 1-2 tuning steps is a natural consequence of trying to maximize the polarimetric sensitivity of the measurements.

Note that the time constant could be much reduced in the  $D_2$  case, since the polarization signals were about 50 times larger. Therefore we do not see any corresponding shift of the  $Q$  profile in the plot for  $D_2$  in Fig. 2.

#### 4.5. Circularly polarized scattering for transverse magnetic fields

Let us now turn to the  $D_1$  case when 100% right-handed circularly polarized incident radiation is used, and Stokes  $I$  and  $V$  are measured in the scattered radiation. The geometry remains the same as in our previous discussion of  $Q$  scattering, with the magnetic field being perpendicular to the scattering plane.

The laboratory measurements were made for a sequence of field strengths between  $\pm 18.7 \text{ G}$ . In Fig. 4 we represent the results as the fractional circular polarization  $V/I$  (%) vs. the strength of the vertically oriented field. In this case  $V$  represents the wavelength integrated  $V$ ,  $I$  the integrated Stokes  $I$  profile. The observations are given by the filled circles and the dashed analytical fit function, while the solid line is obtained with our theory, using the same values for parameters  $\gamma_c$  and  $\tau$  as we used for the modeling of  $Q$  scattering. In contrast to the linearly polarized case, the incident circular polarization leads to radiative couplings between all the initial  $m$  states and not only between those with identical  $m$  quantum numbers, as explained in Sect. 3.3.3.

We notice in Fig. 4 the excellent agreement between the solid and dashed curves, in particular the equal slopes of the field dependence, except for fields in the inner range 0-2 G. The remarkable negative peak is centered at the value 0.43 G (marked by the vertical dotted line in the diagram). This offset from zero can be understood as being caused by the Earth's magnetic field, which has a downwards pointing component of approximately this magnitude. To compensate this component our imposed magnetic field needs to have an upwards (positive component) of this magnitude, which leads to the apparent small shift of our field strength scale.

Since the Earth's magnetic field is not exactly vertical but inclined, the residual field will become horizontal when the vertical field gets compensated, but the azimuth orientation of our experimental setup with respect to the azimuth of this residual horizontal component is not sufficiently known to allow meaningful modeling of this behavior. In the milligauss range in the immediate neighborhood of the +0.43 G offset we can expect the magnetic-field vector to rapidly change its

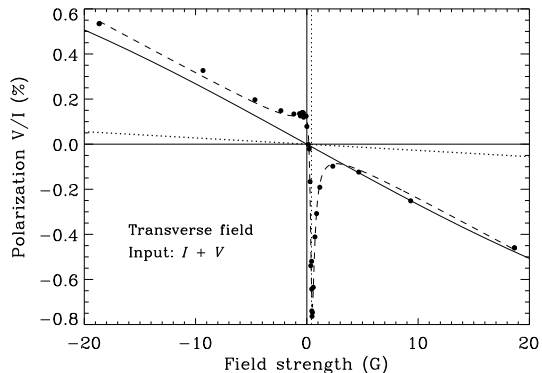


Fig. 4.— Degree of circular polarization in the beam scattered at  $90^\circ$  by potassium  $D_1$ , plotted as a function of field strength. The fractional circular polarization here represents the area of the Stokes  $V$  profile divided by the area of the  $I$  profile. The incident beam has 100% right-handed circular polarization, and the magnetic field is perpendicular to the scattering plane. The observations are represented by the filled circles and the dashed curve, the theoretical model that includes initial and final state coherences by the solid line. When these ground-state coherences are omitted but the interference terms of the excited state are retained, one obtains the dotted line, which has a slope that is an order of magnitude smaller. If all  $m$  state coherences would be omitted the polarization would be exactly zero.

orientation between vertical and horizontal. The sharp negative peak in Fig. 4 shows that the scattering polarization has enormous sensitivity to the field orientation in this milligauss range. The existence of this sharp peak indicates that our description of the physical system is still incomplete. The radiation-matter interaction appears to have a much richer substructure than anticipated.

Other laboratory tests that we have made show that when we have horizontal magnetic fields aligned along the propagation direction of the incident radiation and choose this radiation to be 100% circularly polarized, then not only the scattered Stokes  $V$ , but also the scattered Stokes  $I$ , varies dramatically with the strength of the imposed field. In contrast to the vertical field case, for which Stokes  $I$  is insensitive to field strength, the horizontal field case leads to a Stokes  $I$  that has a sharp peak around zero field strength and rapidly declines towards zero as the field strength increases (Thalmann et al. 2009). This behavior can be readily understood in terms of extreme optical pumping of the medium. With the described geometry either only  $q = +1$  or  $q = -1$  transitions will be excited (depending on the handedness of the incident circular polarization). If for example only radiative excitations that raise the  $m$  quantum number by  $+1$  are possible, then all the atoms of the medium will quickly be pumped into the ground state with  $m = +2$ ,  $F = 2$ , from which no more radiative excitation is possible. This means that the medium becomes transparent and the scattered intensity goes to zero, as observed except for the weak fields around zero. The Stokes  $I$  peak at zero field strength occurs because there are weak stray fields (in particular the Earth’s magnetic field), which break the symmetry and prevent the extreme pumping scenario from happening.

The laboratory experiment was also done with the opposite handedness of the input polarization (100% left-handed circularly polarized radiation). The result is the same, except that the sign of the output  $V/I$  is reversed (and consequently the sharp peak at  $+0.43$  G is positive). The exact sign reversal also happens for the theoretical model, the diagram looks the same if we reflect it in the horizontal axis. This symmetry behavior implies (as verified by our theory) that all the  $V$  signal in the output radiation comes from the non-zero

Mueller matrix element  $M_{44}$ , while the other elements of the 4th row, like  $M_{41}$ , are exactly zero.

In contrast to the scattering of  $Q$  polarization, dichroism does not play any role in Fig. 4. The reason is that the term  $\phi_V$ , which represents the longitudinal Zeeman effect in the Mueller matrix  $\Phi$ , is zero because we have chosen the magnetic field to be transverse. Therefore the effect of the finite optical depth is to multiply both the scattered  $I$  and  $V$  profiles with the same factor,  $\exp(-\phi_I \tau)$ , which differentially suppresses the line core more than the wings. Since it turns out that the scattered  $I$  and  $V$  profiles have identical shapes and thus are deformed in the same way by the factor  $\exp(-\phi_I \tau)$ , the fractional polarization, integrated  $V$  divided by integrated  $I$ , is not affected. This is not so in the  $Q$  scattering case, since the  $I$  and  $Q$  profiles have different shapes, and in addition there is the contribution from  $\phi_Q$ , which is non-zero since it represents the transverse Zeeman effect.

If we would remove the initial and final state coherences but keep the upper-state coherences (like in the standard scattering theory of Eq. (6)), then we obtain the dotted curve in Fig. 4, which has a slope that is an order of magnitude smaller than that of the observations. If we would also remove the upper-state interferences we would get exactly zero for all field strengths. This demonstrates that all the polarization effects in  $V$  scattering for transverse magnetic fields have their origin in coherences between separate magnetic substates, and that the dominating contributions come from coherences in the ground state.

## 5. Limitations, conclusions, and outlook

Our search for missing physics in quantum scattering was motivated by the observed existence of a small but significant polarization peak in the Sun’s spectrum of the NaI  $D_1$  line at 5896 Å. Quantum theory appeared to predict that the  $D_1$  line should be intrinsically unpolarizable, and the transverse Zeeman effect could be ruled out as a source of the observed polarization. After a decade of failed attempts to explain this enigmatic feature we decided to set up a laboratory experiment to address the question whether this was a problem of solar physics or quantum physics.

Quantum systems often contain an inherently

rich and complex structure that is not always fully understood. The correct application of a complex theory needs guidance from experimental data. The problem is that the theory of polarized scattering at multi-level atomic systems has never been experimentally tested before in the parameter range that we are addressing here. This needs to be done before we can have sufficient confidence in the application of the theory to ‘messy’ astrophysical environments over which we have no control.

In most cases when new types of instrumentation allows the exploration of parameter domains that have never been accessed before, surprising new phenomena have been discovered which were not predicted by the theory available at the time. The  $D_1$  enigma was never expected but was a major surprise when the Sun’s spectrum could be recorded with high-precision imaging spectropolarimetry allowing a sensitivity of  $10^{-5}$  in the fractional polarization. Laboratory experiments in polarized scattering was a hot topic in the early days of quantum mechanics but they were largely abandoned around 1935 in favor of other topics. The polarization phenomena that we are discussing here are way out of reach for the experimental technology available at that time.

The aim of our laboratory experiment is not to try to emulate scattering in the solar atmosphere, but to test the basics of  $D_1$  scattering physics under simple and controlled conditions. The experiment revealed that there is indeed a problem of quantum physics:  $D_1$  exhibits a rich polarization structure in situations where available theory predicts zero polarization.

When abandoning the prevailing ‘flat-spectrum approximation’ we open a Pandora’s box to a new world of coherency phenomena that were excluded before. In the present paper we show that polarized scattering theory for multi-level atomic systems has to be extended to include *both* the initial-state *and* final-state coherences (in addition to the coherences in the excited, intermediate state) in order to explain the observed polarization structures. With our phenomenological extension of the theory we succeed in reproducing the observations not only qualitatively in terms of profile shapes and signs, but also quantitatively in great detail, both for the scattering of linear and circular polarization in a transverse field geometry. This

gives us confidence that the missing ingredients of the theory have been identified correctly.

There are however also indications that our theoretical extension is far from complete. Experiments with the scattering of circular polarization indicate that there are dramatic effects happening in the milligauss regime of the external magnetic field (cf. Fig. 4). We are presently unable to deal with this regime, because we lack control and knowledge of the strength and orientation of the field in the milligauss range due to the presence of stray fields, including the Earth's magnetic field. An experiment that could properly deal with this issue is likely to reveal additional substructures of the atomic system that have not been identified so far. To fully address the behavior for such weak fields the experiment needs to be set up in a magnetically clean environment, which is not easy but doable.

Another deficiency is that we only had access to a vapor cell that used argon buffer gas to prevent condensations on the cooler cell windows. As a consequence the potassium atoms experience a high collision rate (with  $\gamma_c \approx 90 \gamma_N$ ), which produce large line broadening and depolarization effects. These effects had to be accounted for in a phenomenological and parametrized way. In future one would like to do the experiment with a cell that does not use any buffer gas, so that one can explore the clean case of scattering in the collisionless domain. In the solar chromosphere, where the core of the NaI D<sub>1</sub> line is formed, one should approach nearly collisionless conditions, but according to Kerkeni & Bommier (2002) lower level polarization in NaI D<sub>1</sub> will always be destroyed under solar conditions. Ideally one would like an experimental setup that would allow exploration of the scattering polarization as a function of collision rate, by being able to change and control the amount of buffer gas being used.

It is generally problematic to apply an established physical theory to parameter domains in which the theory has never been tested by experiment. We do not have a theory that has been sufficiently tested experimentally when it comes to the interpretation of scattering polarization from multi-level atomic systems. Experimental exploration of this poorly studied domain may bring unexpected new insights into neglected aspects of quantum physics. In the present paper we have

tried to indicate the direction in which the exploration of this domain could take us.

The potassium cell was specially tailor made free of charge for our laboratory experiment by the late Alessandro Cacciani, who had devoted much of his life to perfect the art of making such cells for magneto-optical filter systems used in helioseismology and solar magnetometry. The scattering experiment was set up and carried out at ETH Zurich as part of two PhD projects, by Alex Feller and Christian Thalmann. The data bank set up by Thalmann for the collection of his laboratory recordings has served as a resource to guide the theoretical efforts. I am grateful to Svetlana Berdyugina and Dominique Fluri for providing me with their IDL code to calculate the atomic level structure and transition amplitudes in the Paschen-Back regime for the sodium and potassium D<sub>1</sub> – D<sub>2</sub> systems, and to Roberto Casini for various discussions on quantum physics, in particular on the nature of the flat-spectrum approximation.

## REFERENCES

- Bommier, V. 1997a, *A&A*, 328, 706  
Bommier, V. 1997b, *A&A*, 328, 726  
Bommier, V. & Stenflo, J. O. 1999, *A&A*, 350, 327  
Cacciani, A. & Fofi, M. 1978, *Sol. Phys.*, 59, 179  
Cacciani, A., Moretti, P. F., & Rodgers, W. E. 1997, *Sol. Phys.*, 174, 115  
Casini, R., Landi Degl'Innocenti, E., Landolfi, M., & Trujillo Bueno, J. 2002, *ApJ*, 573, 864  
Casini, R. & Manso Sainz, R. 2005, *ApJ*, 624, 1025  
Gandorfer, A. M., Steiner, P., Povel, H. P., et al. 2004, *A&A*, 422, 703  
Hanle, W. 1924, *Z. Phys.*, 30, 93  
Kerkeni, B. & Bommier, V. 2002, *A&A*, 394, 707  
Klement, J. & Stenflo, J. O. 2003, in *Astronomical Society of the Pacific Conference Series*, Vol. 307, *Solar Polarization 3*, ed. J. Trujillo-Bueno & J. Sanchez Almeida, 278  
Landi Degl'Innocenti, E. 1998, *Nature*, 392, 256

- Landi Degl’Innocenti, E. & Landolfi, M. 2004, *Astrophysics and Space Science Library*, Vol. 307, *Polarization in Spectral Lines* (Kluwer)
- Nagendra, K. N., Stenflo, J. O., Qu, Z. Q., & Sampoorna, M., eds. 2014, *Astronomical Society of the Pacific Conference Series*, Vol. 489, *Solar Polarization 7*
- Povel, H. 1995, *Optical Engineering*, 34, 1870
- Povel, H. P. 2001, in *Astronomical Society of the Pacific Conference Series*, Vol. 248, *Magnetic Fields Across the Hertzsprung-Russell Diagram*, ed. G. Mathys, S. K. Solanki, & D. T. Wickramasinghe, 543–552
- Sowmya, K., Nagendra, K. N., Stenflo, J. O., & Sampoorna, M. 2014, *ApJ*, 786, 150
- Stenflo, J. O. 1980, *A&A*, 84, 68
- Stenflo, J. O. 1994, *Solar Magnetic Fields — Polarized Radiation Diagnostics*. (Kluwer)
- Stenflo, J. O. 1998, *A&A*, 338, 301
- Stenflo, J. O. 2004, in *Reviews in Modern Astronomy*, Vol. 17, *The Sun and Planetary Systems — Paradigms for the Universe*, ed. R. E. Schielicke, 269–296
- Stenflo, J. O. 2009, in *Astronomical Society of the Pacific Conference Series*, Vol. 405, *Solar Polarization 5: In Honor of Jan Stenflo*, ed. S. V. Berdyugina, K. N. Nagendra, & R. Ramelli, 3
- Stenflo, J. O. 2011, in *Astronomical Society of the Pacific Conference Series*, Vol. 437, *Solar Polarization 6*, ed. J. R. Kuhn, D. M. Harrington, H. Lin, S. V. Berdyugina, J. Trujillo-Bueno, S. L. Keil, & T. Rimmele, 3
- Stenflo, J. O., Gandorfer, A., & Keller, C. U. 2000a, *A&A*, 355, 781
- Stenflo, J. O. & Keller, C. U. 1996, *Nature*, 382, 588
- Stenflo, J. O. & Keller, C. U. 1997, *A&A*, 321, 927
- Stenflo, J. O., Keller, C. U., & Gandorfer, A. 2000b, *A&A*, 355, 789
- Thalmann, C., Stenflo, J. O., Feller, A., & Cacciani, A. 2006, in *Astronomical Society of the Pacific Conference Series*, Vol. 358, *Solar Polarization 4*, ed. R. Casini & B. W. Lites, 323
- Thalmann, C., Stenflo, J. O., Feller, A., & Cacciani, A. 2009, in *Astronomical Society of the Pacific Conference Series*, Vol. 405, *Solar Polarization 5: In Honor of Jan Stenflo*, ed. S. V. Berdyugina, K. N. Nagendra, & R. Ramelli, 113
- Trujillo Bueno, J., Landi Degl’Innocenti, E., Colados, M., Merenda, L., & Manso Sainz, R. 2002, *Nature*, 415, 403